A Dual-Band Wireless Power Transfer and Backscatter Communication Approach for Implantable Neuroprosthetic Devices

Eleftherios Kampianakis*, Apoorva Sharma*, José Arenas* and Matthew S. Reynolds*†
*Department of Electrical Engineering, University of Washington, USA
†Department of Computer Science and Engineering, University of Washington, USA
Seattle, Washington 98195, USA

***Abstract*—We present a dual-band HF and UHF fully-integrated implantable neuroprosthetic testbed. This testbed includes a custom implanted device as well as an external system based on a commercially available USRP B210 software defined radio (SDR) platform. The implanted device integrates a BPSK backscatter uplink rate of 5 Mbps, an HF WPT efficiency of 47% with a power consumption of 1.332 milliwatt. The implanted device measures 25 mm diameter and has a total thickness of 2.8 mm including the printed circuit substrate, antenna, all circuitry, and silicone encapsulation. It supports up to 10 neural and 4 electromyogram (EMG) channels with a sampling rate of 26.1 kHz for the neural channels and 1.628 kHz for the EMG channels. The communication link is shown to have 0% packet error rate at an implant depth of up to 2.5 cm.**

I. Introduction

IMPLANTABLE neuroprosthetic devices are an area of increasing research interest due to the large number of clinical indications that neuroprosthetics could address. These clinical indications include muscle spasticity and pain [1] seizures, dystonia, severe depression and many others [2]. As a result, numerous research and industry teams are working to implement this new class of bioelectronic devices incorporating amplification, digitization and wireless transmission of neural activity, along with electrical and/or optogenetic stimulation of neurons while tackling significant challenges in the process [3], [4].

Supporting a high channel count of neural inputs is critical for research in neuroprosthetic and brain-computer interface (BCI) applications [5], [6]. However, the number of channels that a system can sample is ultimately constrained by its communication rate. High bandwidth conventional wireless systems (such as IEEE 802.11 / WiFi) that utilize active transmitters consume tens to hundreds of milliwatts and are therefore thermally unfavourable for implanted applications where power dissipation in tissue is limited to the order of 10 mW/cm^3. Since low power dissipation is a critical constraint for implanted systems, various non-traditional communication modalities have been explored. A few examples in the literature include radio frequency (RF) modulated backscatter [7]–[9], backscatter of ultrasound [10] and impulse radio ultrawideband (IR-UWB) transmission [11]. Related to our approach, the authors of [7] achieved a link rate of 30 Mbps using an implantable communication link based on BPSK backscatter modulation in the ultra-high frequency (UHF) ISM band (915 MHz).

978-1-4799-1441-8/13$31.00

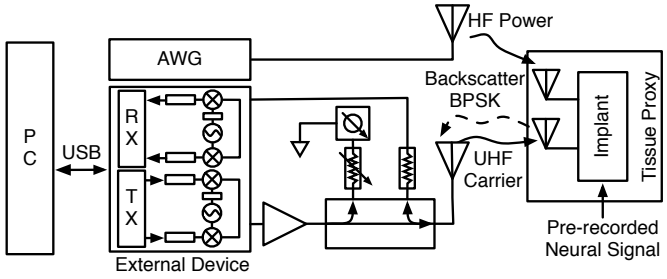

Fig. 1. High-rate implantable communication system testbed.

In addition to the aforementioned communication challenges, power delivery is also a significant issue, especially in chronic (long-term) implanted devices. Wireless power transfer (WPT) using magnetic induction has been widely used for this purpose; [12] and [13] demonstrated high efficiency WPT in the 13.56 MHz industrial, scientific and medical (ISM) band.

One of the most prominent examples of a complete BCI system is demonstrated in [3], [14] where a 64-channel neural recording implantable system is developed that communicates using modulated backscatter. However, the system is limited to 1 Mbps communication rate and as a result their sampling rate is confined to only 1 kHz.

This work aims to combine UHF modulated backscatter communication with HF WPT in a fully integrated implantable system that exhibits both high wireless power transfer (WPT) efficiency and high uplink data rates. The system is a combination of a custom implant device, with a commercial low-cost software defined radio (SDR) platform serving as the external system. A block diagram of this system is shown in Fig. 1. The implanted device is powered by a 13.56 MHz WPT link, and uplinks neural recording data at 915 Mhz using a binary phase shift keying (BPSK) backscatter modulator. The external SDR supplies the communication carrier wave (CW) at 915 MHz and downconverts the backscattered signal

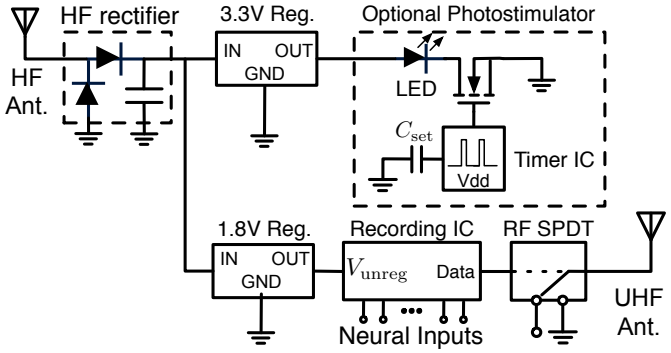

Fig. 2. Implanted device schematic.

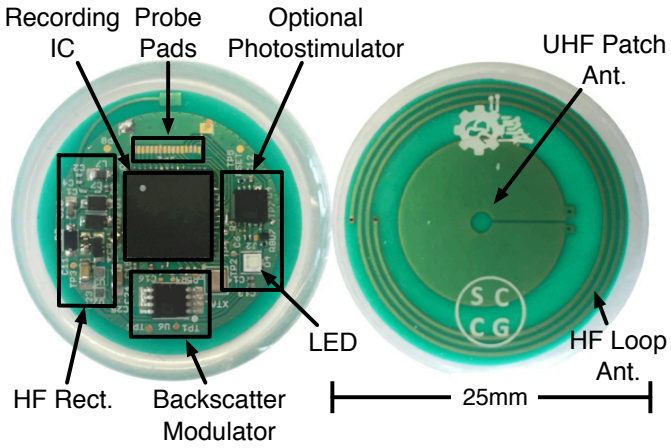

Fig. 3. Implant prototype encapsulated in biocompatible silicone.

to provide a host PC with baseband I/Q samples for software demodulation using Gnuradio and Matlab. An external self-jammer cancellation network suppresses the reflected carrier energy to greatly improve receiver sensitivity. To the best of our knowledge, this is the first demonstration of a complete backscatter-based implantable system operating at a data rate of 5 Mbps or greater, including an off-the shelf external system, HF WPT, and offering multi-channel neural and electromyography (EMG) recording.

II. Implant Design

A schematic of the envisioned system is depicted in Fig. 2. A dual-band antenna that was utilized in [15] receives the incoming HF carrier, which is rectified and regulated to provide power to the implant. A previously developed neural recording integrated circuit (IC) [8] is used to digitize up to a total of 10 neural and 4 EMG inputs, and is responsible for driving the SPDT RF switch that implements the BPSK backscatter modulation. Finally, the capability for optogenetic photostimulation is available through a custom circuit that provides pulse width modulation (PWM) control of a miniature blue light emitting diode (LED).

The antenna and the implant components are encapsulated in a biocompatible silicone polymer (Dow Corning MDX4-4120). The encapsulation procedure uses centrifugation and vacuum curing to remove air bubbles and ensure a tight bond to the circuit. The implant prototype measures 25 mm diameter and a total thickness of 2.8 mm including the substrate, antenna, all circuitry, and biocompatible silicone encapsulation as depicted in Fig. 3.

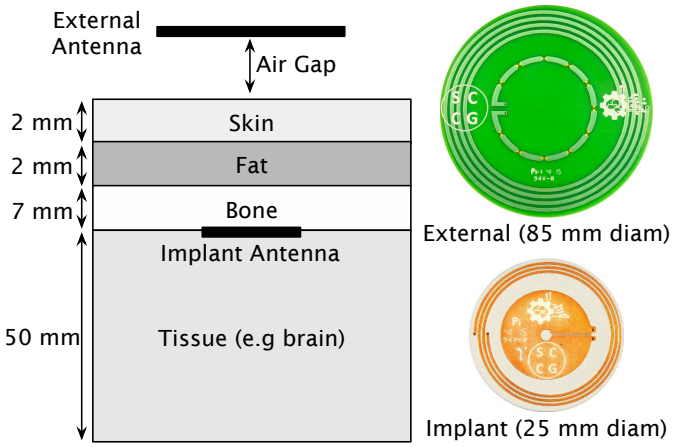

Fig. 4. Implant antenna model used for simulations, from [15].

A. Dual-Band Antenna Subsystem

The implant antenna subsystem was developed in [15] and consists of a 25 mm diameter implant antenna and a 85 mm diameter external antenna. The antenna system has been previously tested in saline tissue proxy as well as in vitro animal tissue. The antenna boards and the simulation model that was utilized are depicted in Fig. 4. In a saline tissue proxy and at an implant depth of 11 mm and an air gap of 5 mm the measured HF power link efficiency is on the order of 17% and the insertion loss of the UHF communication link is on the order of 38 dB.

The choice of the ISM HF band for the power link was made because the frequency of 13.56 MHz provides a satisfactory efficiency with a relatively small antenna size. Moreover, high data rates are required, hence the ISM UHF band of 915 MHz was utilized due to the broad spectrum of (26 MHz) that is available at this particular band.

B. HF Wireless Power Transfer Receiver

A voltage doubling rectifier was utilized in order to convert the incoming HF WPT carrier at 13.56 MHz from the external system into direct current (DC) power. The output of the rectifier is regulated using low-dropout (LDO) regulators to provide 3.3V and 1.8V rails. Significant effort was invested in component selection for small form factor, low power consumption, and over-voltage tolerance. Schottky diodes (1N5711, Diodes Incorporated) were utilized due to their high reverse voltage rating of 70 V as well as their low forward voltage drop of 410 mV. Voltage regulators from the Texas Instruments (TI) LP5907 series were selected. A 3.3 V regulator powers the photostimulator and a 1.8 V regulator powers the recording IC. This regulator series was selected due to its package size

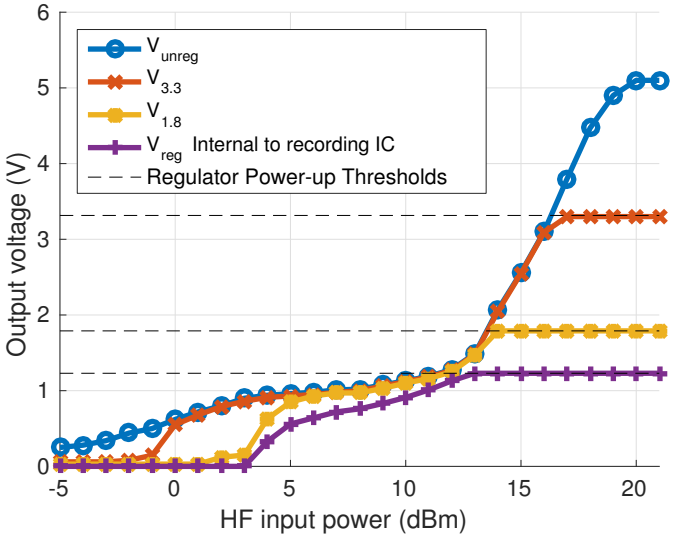

Fig. 5. Regulator outputs vs HF input power. The implant powers-up at an input power of 13 dBm and the optional photostimulator circuit at 17 dBm.

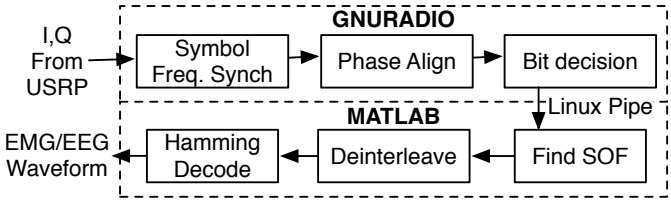

Fig. 6. Receiver pipeline.

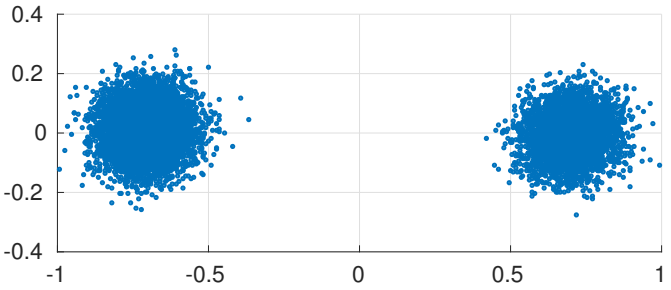

Fig. 7. I/Q samples after the phase-alignment PLL. The sample are synchronized in terms of symbol frequnecy and aligned in phase with the I/Q plane.

of only 0.65 x 0.65 mm and low dropout voltage of 120 mV. Most importantly, these regulators have an unusually high power supply rejection ratio (PSRR) at 13.56 MHz, that was measured at approximately 20 dB. This specification is critical in order to reduce the unwanted residual 13.56 MHz ripple coming from the rectifier. Generally speaking, the PSRR of an LDO regulator will be very high at frequencies within the loop bandwidth of the regulator (50 dB or more, for frequencies up to e.g. 100 kHz), but for most commonly available LDOs, the PSRR decreases to near zero at frequencies of 1 MHz or above.

In order to achieve maximum performance from the rectifier, proper matching to the antenna is necessary. The matching component values were calculated with the following procedure: the total DC power consumption of the system was measured and found to be 0.74 mA at 1.8 V (with the photostimulator disabled). A 2432 Ω load was therefore connected to the output of the LDO to emulate the system power consumption. The return loss ($|S11|$) at the rectifier input (prior to matching) was measured at 13.56 MHz over a range of input powers. The minimum $|S11|$ designated the operating point of the system and the S11 value was used to calculate the corresponding components for a conjugate match. After matching, the rectifier exhibits 47% efficiency at this operating point. This is very close to the theoretical 50% efficiency that can be achieved with a conjugate match.

The HF WPT system was tested over different input powers in a saline tissue proxy, with 1 cm implant depth and with the external antenna having an air gap of 0.5 cm. Fig. 5 depicts the output of the rectifier and the different board-level and chip-level supply voltages. The HF input power at the external antenna port for which the LDOs enter regulation are as follows:

- Recording IC, integrated 1.23 V LDO: +13 dBm.
- TI 1.8 V LDO: +14 dBm.
- TI 3.3 V LDO: +17 dBm.

Thus a minimum HF drive power of +17 dBm must be supplied under these implant conditions. A 5.1 V Zener diode is integrated into the rectifier circuitry (not shown in Fig. 2) to protect the implant from excess HF power.

III. External System

The commercial off-the-shelf (COTS) external system is depicted in Fig. 8. It is based on an Ettus Research, Inc. USRP B210 which is connected to an added RF front-end that consists of an additional power amplifier and a self-jammer cancellation subsystem.

A. Software defined radio subsystem

The USRP B210 is a low cost ($1100) software defined radio supporting carrier frequencies of $70 - 6000$ MHz, with baseband bandwidth up to 56 MHz. In our system, the USRP B210 is responsible for supplying the UHF communication carrier at 915 MHz and receiving the backscatter subcarriers containing uplink data from the implant. The USRP is connected to a PC with USB 3.0 to control the USRP and convey the baseband data to the PC. GNUradio, an open source, block-based signal processing software was utilized. A custom GNURadio flowgraph was designed that sets up the USRP hardware at a baseband sampling rate of 20 Msps and processes the incoming I/Q symbols in real-time.

Fig. 6 depicts a simplifed view of the GNURadio receiver pipeline that we implemented. First, a phase locked loop (PLL) that exploits poly-phase filter banks [16] locks to the backscattered symbol frequency and downsamples accordingly. Next, another PLL that exploits the Costas-loop architecture [17] shifts the phase of the symbols on the I/Q plane in so that

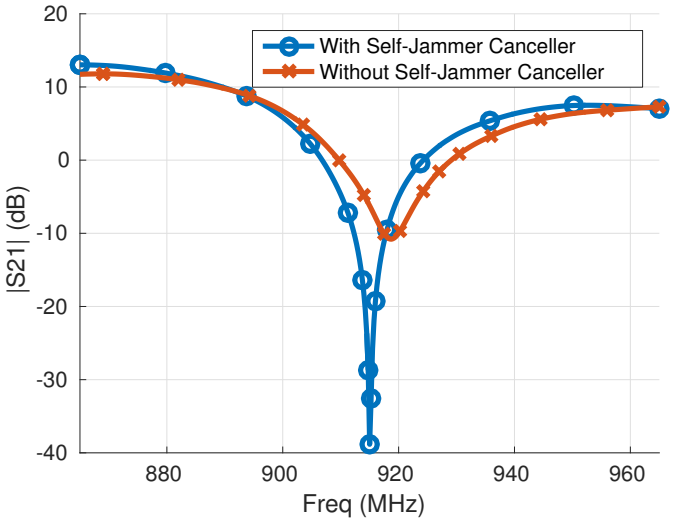

Fig. 9. Measured self-jammer carrier suppression ratio with and without the self-jammer cancellation circuit. The self-jammer canceller reduces the carrier amplitude by $\approx$ 39 dB.

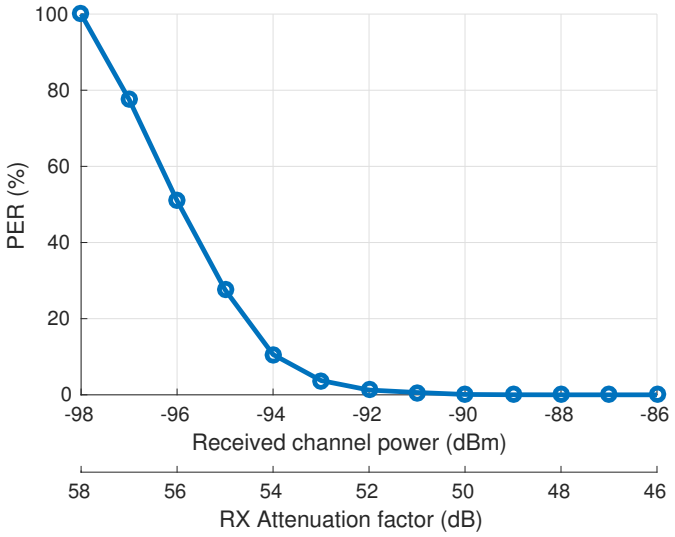

Fig. 10. Packet error rate vs. receive-path attenuation factor and corresponding absolute channel power.

slicing can be implemented simply by checking the sign of each sample. Followingly, a bit decision block outputs the demodulated bits.

The PC that runs the demodulating software employs 16 GB of RAM and an Intel Core-i7 processor clocked at 3.8 GHz. It is important to note that for rates up to 1.5 Mbps, a Linux pipe can be utilized and the output of the flowgraph can be processed in near-real time from MATLAB using batch processing of 3000 frames at a time. Fig. 7 depicts an I/Q plot of 10000 samples that were collected after the the phase alignment block. The symbols were generated at a rate of 5 Msps using the recording IC and then collected by the USRP-based external system.

The MATLAB script is responsible for post-processing the data generated by the GNURadio flowgraph. Start-of-frame (SOF) synchronization is performed with the utilization of the Barker codes that are embedded in the data stream transmitted by the recording IC [8]. After frame synchronization, de-interleaving is performed to extract the 16-bit blocks containing the digitized neural/EMG data. The last step is a Hamming $(16, 11)$ decoder that provides single error correction, double error detection (SECDED) functionality to extract the 11-bit neural/EMG samples.

B. RF interface

A Mini-Circuits ZRL-3500 amplifier increases the carrier power generated by the USRP up to $+25$ dBm. The output of the amplifier is connected to a self-jammer cancellation circuit as shown in Fig 1. The latter is comprised of a Mini-Circuits ZX30-20-20BD+ 10 dB directional coupler, a Weinschel 980-2K variable phase shifter (having 100 degrees phase shift range) and a JFW 50R-019 1 dB step attenuator with 0-10 dB attenuation range. With careful adjustment of the phase shifter and the attenuator, the signal that exits the output coupling port contains the backscattered signal with a carrier suppression of up to $\approx$ 39 dB as shown in Fig. 9. Similar directional coupler based self-jammer suppression networks can be found in [18], [19].

To provide the HF carrier that powers the implant, an Agilent 3350B arbitrary waveform generator (AWG) was utilized. The output HF power at 13.56 MHz can be provided up to $+23$ dBm, but as previously described, only +17 dBm is required at an 1 cm implant depth, with the external antenna having an air gap of 0.5 cm.

IV. Measurement Results

As shown in Fig. 8, benchtop testing employs a 3D-printed fixture allowing the adjustment of the air gap between the external antenna and the saline tissue proxy (0.91% w/v saline solution). The transmit antenna is placed beneath a styrofoam cup that contains the saline solution, and this fixture is placed in a Faraday cage in order to shield the experiment from external interference.

A. Sensitivity/Range characterization

To characterize the performance of the backscatter communication link, the benchtop setup with an air gap of 0.5 cm, an implant depth of 1 cm and a saline water height of 6 cm was utilized. The in-channel power of the backscattered subcarrier was first measured with a signal analyzer at the output-coupled port of the directional coupler. With a $+25$ dBm carrier power from the external system, the received channel power was measured and found to be -40 dBm. Variable attenuation in the receive path was used to reduce the available subcarrier power.

Packet error rate (PER) measurements were first made as a function of available channel power by counting cyclic redundancy check (CRC) errors, after Hamming decoding from 25000 packets for different RX attenuation factors. Fig. 10

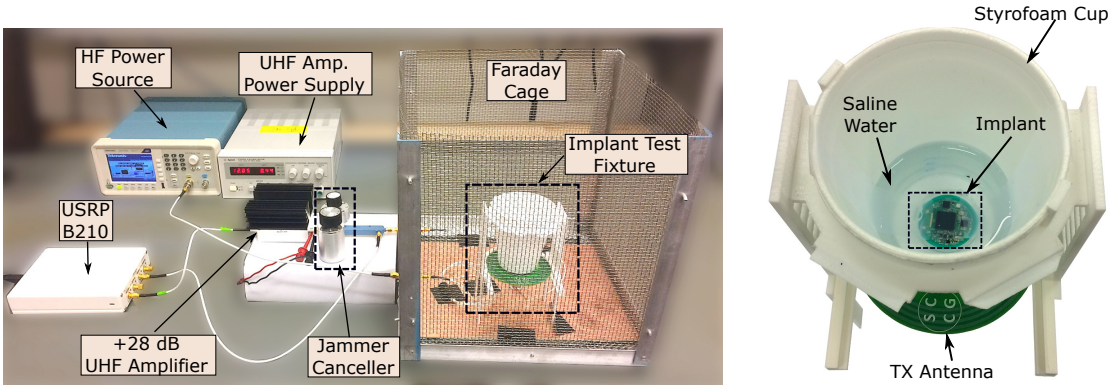

Fig. 8. Left: Implanted communication system testbed. Right: 3D-printed fixture for varying the air-gap and implant depth.

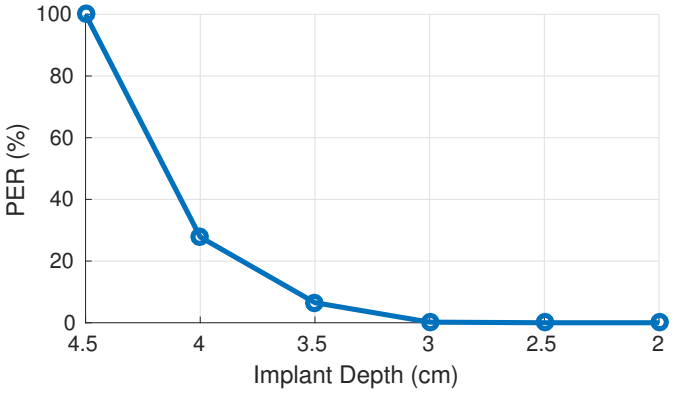

Fig. 11. PER vs implant depth with a fixed UHF carrier power level of 0 dBm.

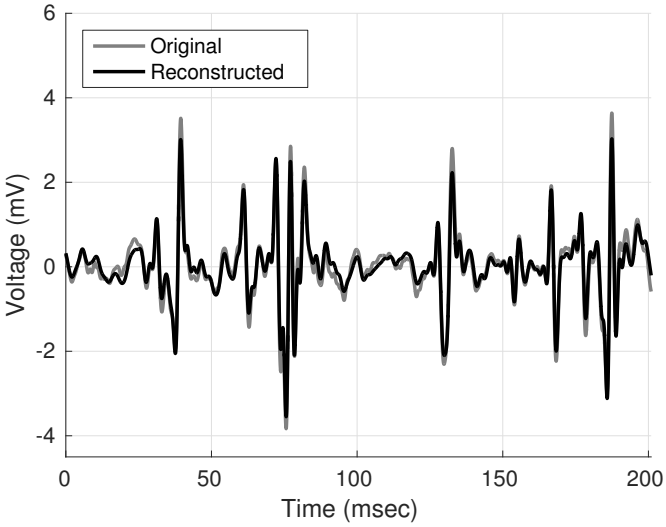

Fig. 12. Original vs reconstructed EMG signal. The reconstructed signal exhibits an RMSE of 189μV.

depicts the corresponding results. The receiver exhibits a PER of under 0.62 % for an input channel power of -91 dBm.

The system was also characterized for PER as a function of implant depth. In this experiment, the externally supplied carrier power was set to 0 dBm, and the PER was measured using the same method as implant depth was varied, with a fixed air gap of 0.5 cm. Fig. 11 depicts the corresponding results. We observed that the backscatter uplink exhibits a PER of better than 0.19 % at an implant depth of up to 3 cm. Less carrier power is better for reducing the specific heat absorption rate (SAR) and the system's overall power consumption. Hence, a carrier power of 0 dBm was utilized for this experiment since it yields a sufficient implant depth. It is important to note that time-domain simulations provided a peak UHF SAR value of 0.457 W/kg averaged over 1 g of mass [15]. This peak SAR value is 3.5 times lower than the regulatory limit of 1.6 W/kg.

B. EMG measurements

Finally, the implanted device was characterized in terms of its biosignal digitization and transfer capability. For this experiment, a pre-recorded electromyogram (EMG) signal was fed into the implant from an arbitrary waveform generator, using an electrode simulator network. A total of 2 seconds of pre-recorded data that were bandpass-filtered at the band of 30-501 Hz, from existing electromyograms [20] were reproduced by an Agilent 33500B series AWG.

A representative portion of the time-domain reconstructed waveform is shown in Fig. 12. The input-referred noise is on the order of 189 μV root mean square (RMS). The recording IC has a previously measured input-referred noise of 43 μV RMS. The increased noise observed in this experiment is due to unwanted coupling of the relatively strong HF WPT signal that is parasitically coupled to the EMG inputs. We believe this noise elevation can be reduced easily with better attention to PC board layout as well as including a simple R-C low-pass network at the inputs to the recording IC.

V. Conclusion and Future Work

We present a dual-band HF and UHF fully-integrated implantable neuroprosthetic testbed. This testbed includes a custom implanted device as well as an external system based

on a commercially available USRP B210 software defined radio (SDR) platform. The implanted device integrates a BPSK backscatter uplink rate of 5 Mbps, an HF WPT efficiency of 47%, power consumption of 1.332 mW. The implanted device measures 25 mm diameter and has a total thickness of 2.8 mm including the printed circuit substrate, antenna, all circuitry, and silicone encapsulation. It supports up to 10 neural and 4 electromyogram (EMG) channels with a sampling rate of 26.1 kHz for the neural channels and 1.628 kHz for the EMG channels. The communication link is shown to have 0% packet error rate at an implant depth of up to 2.5 cm. Future work includes noise mitigation via a revised PC board layout as well as including a simple R-C low-pass network at the inputs to the recording IC. Further in vitro testing will be conducted to ensure both neural and EMG recording performance before commencing *in vivo* work with animals such as rodents and non-human primates. Additional work includes development of higher communication rate implants by exploiting higher order backscatter, such as QAM modulated backscatter [21].

ACKNOWLEDGMENT

The project described was supported in part by Award Number EEC-1028725 from the National Science Foundation. The content is solely the responsibility of the authors and does not necessarily represent the official views of the National Science Foundation.

REFERENCES

[1] N. Bhadra and K. L. Kilgore, "High-Frequency Electrical Conduction Block of Mammalian Peripheral Motor Nerve," *Muscle & Nerve*, vol. 32, no. 6, pp. 782–790, 2005.

[2] K. Birmingham, V. Gradinaru, P. Anikeeva, W. M. Grill, V. Pikov, B. McLaughlin, P. Pasricha, D. Weber, K. Ludwig, and K. Famm, "Bioelectronic medicines: a research roadmap," *Nature Reviews Drug Discovery*, vol. 13, no. 6, pp. 399–400, 2014.

[3] M. M. Maharbiz, R. Muller, E. Alon, J. M. Rabaey, and J. M. Carmena, "Reliable Next-Generation Cortical Interfaces for Chronic Brain-Machine Interfaces and Neuroscience," *Proc. of the IEEE*, vol. 105, no. 1, pp. 73–82, Jan 2017.

[4] N. M. Neihart and R. R. Harrison, "Micropower Circuits for Bidirectional Wireless Telemetry in Neural Recording Applications," *IEEE Trans. Biomed. Eng.*, vol. 52, no. 11, pp. 1950–1959, Nov 2005.

[5] P. Ledochowitsch, A. C. Koralek, D. Moses, J. M. Carmena, and M. M. Maharbiz, "Sub-mm functional decoupling of electrocortical signals through closed-loop bmi learning," in *Proc. IEEE Eng. Med. Biol.*, Jul. 2013, pp. 5622–5625.

[6] S. Ha, A. Akinin, J. Park, C. Kim, H. Wang, C. Maier, P. P. Mercier, and G. Cauwenberghs, "Silicon-Integrated High-Density Electrocortical Interfaces," *Proc. of the IEEE*, vol. 105, no. 1, pp. 11–33, Jan 2017.

[7] J. S. Besnoff and M. S. Reynolds, "Near field modulated backscatter for in vivo biotelemetry," in *Proc. 2012 IEEE Intl Conf. RFID (RFID 12)*, Apr. 2012, pp. 135–140.

[8] S. J. Thomas, R. R. Harrison, A. Leonardo, and M. S. Reynolds, "A Battery-Free Multichannel Digital Neural/EMG Telemetry System for Flying Insects," *IEEE Trans. Biomed. Circuits Syst.*, vol. 6, no. 5, pp. 424–436, Oct 2012.

[9] J. Charthad, M. J. Weber, T. C. Chang, and A. Arbabian, "A mm-Sized Implantable Medical Device (IMD) With Ultrasonic Power Transfer and a Hybrid Bi-Directional Data Link," *IEEE J. Solid-State Circuits*, vol. 50, no. 8, pp. 1741–1753, Aug 2015.

[10] D. Seo, R. M. Neely, K. Shen, U. Singhal, E. Alon, J. M. Rabaey, J. M. Carmena, and M. M. Maharbiz, "Wireless Recording in the Peripheral Nervous System with Ultrasonic Neural Dust," *Neuron*, vol. 91, no. 3, pp. 529–539, 2016.

[11] H. Ando, K. Takizawa, T. Yoshida, K. Matsushita, M. Hirata, and T. Suzuki, "Wireless Multichannel Neural Recording With a 128-Mbps UWB Transmitter for an Implantable Brain-Machine Interfaces," *IEEE Trans. Biomed. Circuits Syst.*, vol. 10, no. 6, pp. 1068–1078, Dec 2016.

[12] A. P. Sample, D. T. Meyer, and J. R. Smith, "Analysis, Experimental Results, and Range Adaptation of Magnetically Coupled Resonators for Wireless Power Transfer," *IEEE Trans. Ind. Electron*, vol. 58, no. 2, pp. 544–554, Feb 2011.

[13] X. Li, C. Y. Tsui, and W. H. Ki, "A 13.56 MHz Wireless Power Transfer System With Reconfigurable Resonant Regulating Rectifier and Wireless Power Control for Implantable Medical Devices," *IEEE J. Solid-State Circuits*, vol. 50, no. 4, pp. 978–989, April 2015.

[14] R. Muller, H.-P. Le, W. Li, P. Ledochowitsch, S. Gambini, T. Bjorninen, A. Koralek, J. M. Carmena, M. M. Maharbiz, E. Alon, and J. M. Rabaey, "A Minimally Invasive 64-Channel Wireless μECoG Implant," *IEEE J. Solid-State Circuits*, vol. 50, no. 1, pp. 344–359, 2015.

[15] A. Sharma, E. Kampianakis, and M. S. Reynolds, "A Dual-Band HF and UHF Antenna System for Implanted Neural Recording and Stimulation Devices," *IEEE Antennas Wireless Propag. Lett.*, 2016.

[16] T. W. Rondeau, V. Shelburne, and V. OShea, "Designing Anaylsis and Synthesis Filterbanks in GNU Radio," in *Karlsruhe Workshop on Software Radios*, 2014.

[17] J. P. Costas, "Synchronous Communications," *Proc. IRE*, vol. 44, no. 12, pp. 1713–1718, Dec. 1956.

[18] J. Carrick, R. Herold, M. Reynolds, Y. Maguire, and R. Pappu, "Methods and Apparatus For Self-Jamming Suppression In A Radio Frequency Identification (RFID) Reader," U.S. Patent 20 100 069 011, Mar. 18, 2010.

[19] J. Y. Jung, C. W. Park, and K. W. Yeom, "A Novel Carrier Leakage Suppression Front-End for UHF RFID Reader," *IEEE Trans. Microw. Theory Techn.*, vol. 60, no. 5, pp. 1468–1477, May 2012.

[20] R. Seward. Examples of electromyograms. [Online]. Available: https://physionet.org/physiobank/database/emgdb/

[21] S. Thomas and M. S. Reynolds, "QAM Backscatter for Passive UHF RFID Tags," in *Proc. 2010 IEEE Intl. Conf. RFID (RFID 10)*, April 2010, pp. 210–214.